Materials Science & Engineering A 690 (2017) 259–269

Contents lists available at ScienceDirect

Materials Science & Engineering A

journal homepage: www.elsevier.com/locate/msea

Natural aging on Al-Cu-Mg structural hardening alloys – Investigation of two historical duralumins for aeronautics

A. Cochard[a], K. Zhu[b], S. Joulié[a], J. Douin[a], J. Huez[b], L. Robbiola[c], P. Sciau[a], M. Brunet[a,*]

[a] CEMES, CNRS, Université de Toulouse, 29 rue Jeanne Marvig, BP 94347 31055 Toulouse Cedex 4, France
[b] CIRIMAT, INP Toulouse, CNRS, 4 allée Emile Monso, 31030 Toulouse, France
[c] TRACES, Université de Toulouse, CNRS, Maison de la Recherche, 5 Allées A. Machado, 31058 Toulouse Cedex, France

ARTICLE INFO

Keywords:
Aluminum alloys
Aging
Precipitation
Electron microscopy
Mechanical characterization

ABSTRACT

This article presents the metallurgic study of sixty years old structural hardening Al-Cu-Mg alloys recovered from a double-deck aircraft Breguet 765. This study aims to characterize and understand the evolution of alloys over very long periods thanks to an approach coupling materials characterization and archives researches. The focus is made on two ancient age hardening Al-Cu alloys: A-U4G and A-U4G1, whose compositions are close to the international designations 2017A and 2024 respectively. Multi-scale structural investigation was carry out and mechanical properties were extracted. It is shown that despite natural aging during long periods, these alloys exhibit mechanical properties (yield strength, ultimate tensile strength and rupture strain) close to the expected original specifications.

1. Introduction

Characterization of the long-term behavior of materials exposed to complex environmental conditions is of great challenge, especially in aeronautics industry where failure can cause irremediable damages. Aluminum alloys are particularly concerned as they constitute the majority of aircraft structures. Developed since the beginning of the 20th century up to now, Al-Cu-Mg alloys or duralumins can be considered as relatively recent metallic materials. Their good mechanical properties are obtained thanks to age or precipitation hardening. The metallurgical process behind hardening consists in heat treating near solvus temperature the Al-Cu-Mg alloy, quenching it in water then performing an aging treatment. The nanoscale precipitation responsible for the hardening of the material occurs at this step. Aging was done originally by maintaining the alloy at room temperature for several days (natural aging or equivalent T3 and T4 treatments). Other treatments can now be found consisting in heating the products between 150 and 200 °C for several hours up to tens of hours (artificial aging or T6 and T8 treatments) to reach the maximum hardness and tensile strength, *i.e.* peak aging [1]. The precipitation sequences in various alloys and the influence of the process conditions on the microstructure and the mechanical properties are well documented [2].

However, the long-term behavior of these alloys when exposed to real environmental conditions during the lifespan of an aircraft remains to be fully understood. Accelerated tests such as creep and high-temperature fatigue or exposure to corrosive environment have been developed to identify degradation mechanisms and consequently to assess long-term aging [3]. Elevated temperature exposure under applied stress is known to introduce changes in the microstructure such as growth of new phases, changes in dislocation density, distribution or grain-boundary precipitation, which influence largely the mechanical properties [3–6]. In order to be closer to reality, application of low temperature ranges and long times is a first approach to model long-term aging. For instance, studies were published where heat was applied on age-hardening alloys for up to two months at temperatures between 100 and 150 °C [6] or up to 8 months (5800 h) at 85 °C [7]. In these two cases, the effect on tensile properties was proved not significant. Accelerated corrosion exposure tests have also been applied for these alloys [6–9] to study the impact on the microstructure and the residual mechanical properties.

Although fully justified and helpful for assessing the materials behavior requested by the aircraft industry, accelerated tests, which simulate long-term service usage, do not represent the exact real aging [3,10]. They also take insufficiently into account the synergistic effects corresponding to complex conditions encountered during aircraft service, which include indeed many factors such as temperature, pressure, loads, pollution or relative humidity. All the combined factors lead to fatigue damage accumulation, which is hard to predict.

This work aims at characterizing aeronautic materials naturally aged on an aircraft. More precisely, two Al-Cu-Mg industrial alloys

* Corresponding author.
E-mail address: magali.brunet@cemes.fr (M. Brunet).

http://dx.doi.org/10.1016/j.msea.2017.03.003
Received 7 September 2016; Received in revised form 1 March 2017; Accepted 2 March 2017
Available online 03 March 2017
0921-5093/

were sampled on an airplane Breguet dating back from the 1950's. These materials, corresponding to the French AFNOR designation A-U4G and A-U4G1 used at the time, are typical structural hardening alloys used in aeronautical industry at this period in Western Europe. A-U4G would be close to the 2017A alloy according to the international designation system in use nowadays [11]. A-U4G1 would be close to the current 2024 alloy and still employed for some parts of aircrafts fuselage skin. They were submitted to the lifespan of the aircraft and outdoor exposure during several decades. Thanks to the restoration of the aircraft, the opportunity to collect specific pieces was offered. These materials represent models for studying long-term aging in real conditions. Information on mechanical properties durability and microstructural evolution that includes very slow physical mechanisms may be extracted.

This investigation of industrial heritage samples is a direct continuation of a previous study focused on aluminum rivets [12]. It requires a detailed methodology coupling materials science and archive historical researches. Indeed, original state of the aged materials cannot be measured directly and the only way to study it is, indirectly, through information collected in technical documents contemporary of the aircraft construction. Comparison with modern alloys can be made but with care as composition may have evolved over the years (impurity levels for instance), which can affect their microstructure and their properties.

After the presentation of the method integrating the sampling strategy, the characterization of materials will be reported. Multi-scale structural investigation, as well as mechanical properties based on tension and microhardness testing have been carried out. The results are compared to data obtained from ancient scientific literature and from technical (R & D) archives of the airplane constructor. The discussion section proposes some hypothesis on the aging state of the sampled alloys.

2. Materials and methods

2.1. Materials

The studied materials were sampled on a 60 years old Breguet Sahara 765 “Deux-Ponts” (Double-Decker) under renovation at the association “Ailes Anciennes Toulouse” in Blagnac, France. The plane flew from 1959 until 1969 [13], after which it was grounded, first on the military base of Evreux, France, then in Blagnac. The aircraft thus experienced two periods of lifetime: 10 years of air service and about 47 years at rest in outdoor condition. Such a long period in outdoor conditions gave rise to severe damages including corrosion on the skin and structural elements. During one of the restoration operations involving metal replacements, two original metallic plates were selected and collected after their removal from this ancient aircraft (Fig. 1). Both plates have a thickness close to 2 mm. They are rolled products, commonly used for fuselage skin and stringers [14]. The first one, called L8 is a large flame-shield plate located inside the engine nacelle. The second one, called L2, is a stringer, located underneath the floor, and acts as a reinforcement at the back of the aircraft.

2.2. Methods

Investigation of these industrial heritage materials requires an adapted methodology, which involves at the same time archives research to extract information on original pieces (nature, role, expected properties) and classical metallurgical study on sampled materials hereafter described.

2.2.1. Chemical composition

The two plates L2 and L8 were first analyzed to determine the nominal composition of the alloys. Chemical analysis was performed by Inductively Coupled Plasma – Optical Emission Spectrometry (ICP-OES) by Evans Analytical Group SAS. Table 1 gives the measured elemental composition of each plate and for comparison, the expected compositions for the same alloys from the French standard AIR 3350/C of 1957 [15]. This standard was applied by the Breguet Company at this period, as it is confirmed in the standards for this aircraft [16].

L8 plate contains less magnesium (0.83 wt%) than L2 (1.53 wt%), which shows that L8 is made of A-U4G alloy whereas L2 is made of A-U4G1 alloy. For the series of Breguet 765 Sahara aircrafts, technical clauses and recovered plans indicate that A-U4G and A-U4G1 were indeed planned for the fuselage skin and structure [17]. It must be recalled that these two alloys, with their high specific strength properties, belong to the Duralumin family. They are age hardened aeronautic alloys, commercialized since 1909 for A-U4G [18] and at the beginning of the 1930s for A-U4G1 [19]. The latter contains a higher magnesium content to improve the tensile strength. A-U4G and A-U4G1 have a composition close to the currently available commercial alloys designated respectively as 2017A and 2024, but with a difference in impurities concentration (Si and Fe). Additional analyses performed by Glow Discharge Mass Spectrometry (GDMS) revealed that the L2 alloy also contains markedly less impurities elements (Zn, Cr, Ti, Ni, Pb, Ga) than the L8 plate.

2.2.2. Structural characterization

In order to observe the metallurgical structure including the different phases distribution, the plates were cut along three perpendicular directions. The directions of cut were: (D1) expected rolling direction, (D2) transversal to rolling surface direction and (D3) thickness direction corresponding to usual Normal Direction (ND). Rolling direction (RD) was hypothesized after preliminary optical observation of cross-sections.

The microstructure was determined from optical and scanning electron microscopies. The plate samples were prepared as usually for metallographic examination. Each specimen was embedded in an epoxy resin and mechanically polished on water-lubricated abrasive papers (silicon carbide) of decreasing granulometry and then on polishing cloths with diamond pastes down to 1 μm particle size. Optical observation was conducted on an inversed microscope Nikon MA200. Etching with Keller's solution (HF 1 ml, HNO_3 2.5 ml, HCl 1.5 ml in demineralized H_2O 95 ml) was applied revealing the microstructure of the alloy and allowing grain shape and size to be measured with linear intercept method.

Examination with scanning electron microscope (SEM) on a JEOL JSM 6460 LV operating at 20 kV and equipped with an Oxford INCA PentaFETx3 energy dispersive X-ray spectrometer (EDS) was performed. Large precipitates ($> 2\ \mu m^2$) were identified and quantified using pure K-line Al, Si and Fe standards. Results were normalized to 100 wt%.

In order to observe the nanostructure and precipitation at this scale, the plates were also cut according to the three directions (D1, D2, D3). After mechanical polishing up to 2400 SiC paper grade, in order to obtain a thickness of 25 μm, the specimens were then electrochemically thinned using a Tenupol-5 Struers apparatus operating at 60 V in a solution of methanol and nitric acid (3:1) at −15 °C. The nanostructure was observed using a Transmission Electron Microscopy JEOL 2010 operating at 200 kV. Chemicals elements presents in some precipitates were identified with a CM20 FEG TEM/STEM microscope, operating at 200 kV and equipped with an energy dispersive X-ray spectroscopy (Quantax EDS system with silicon drift detector, from Bruker).

2.2.3. Mechanical testing

Tensile specimens were cut in each plate: 6 in D1 direction and 6 others in D2 direction (perpendicular to D1) allowing to get a representative set of data in order to evaluate a possible dispersion of the results for these two surface directions. As depicted in Fig. 2, the gauge length/reduced section and width of the tensile specimen are 20 mm and 3 mm respectively. The gauges were polished mechanically

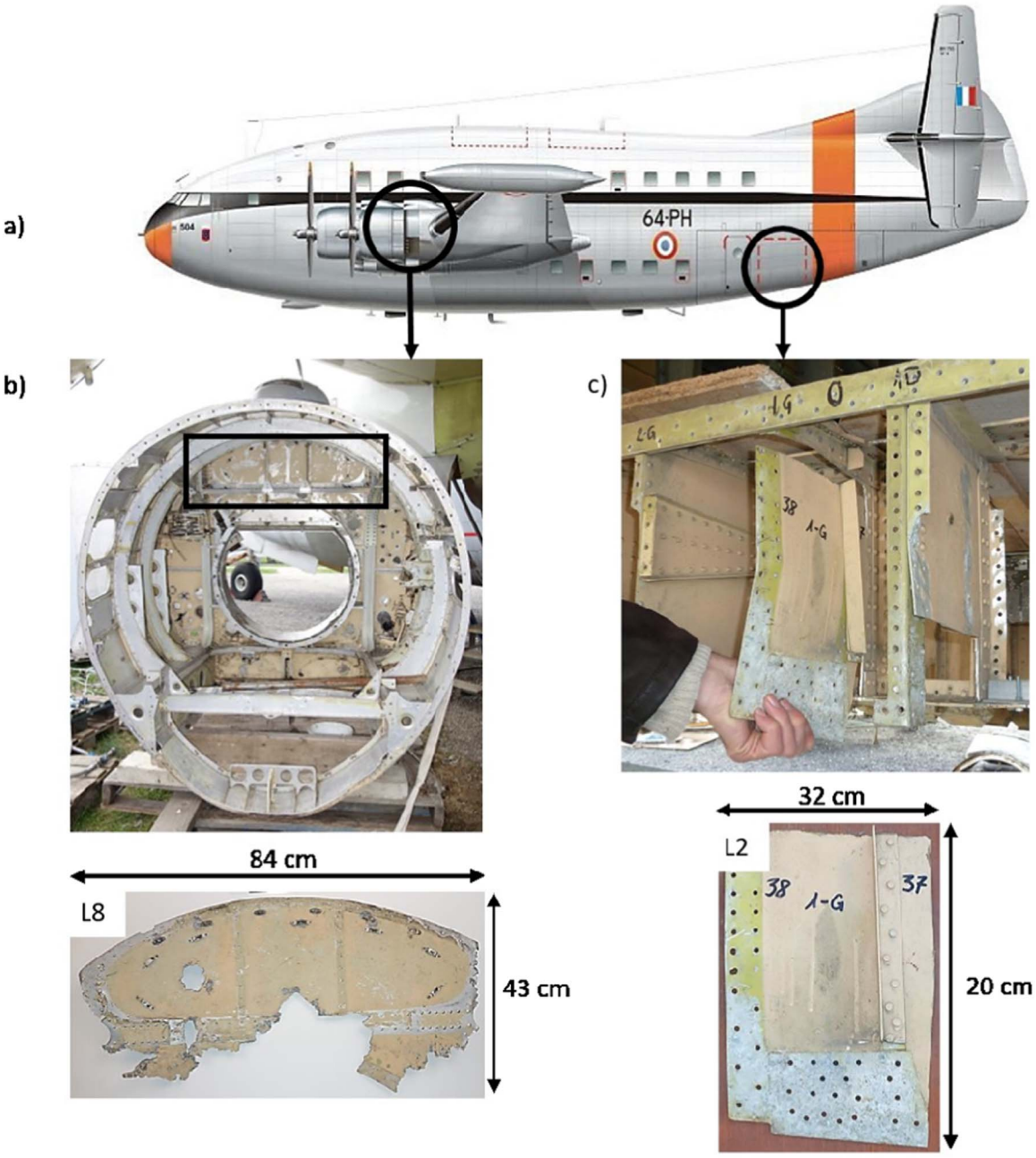

Fig. 1. (a) Presentation of the Breguet 765 aircraft, source: ©Olivier Beernaert at http://www.traditions-air.fr; and the two samples location (b) L8, a plate located in the left engine nacelle; (c) L2, a plate located underneath the first stage, into the plane.

Table 1
Elemental composition in wt% of sampled aeronautic plates, obtained by ICP-OES, compared to 1954 literature data: standard Air 3350/C [15] and current international standard by The Aluminum Association [11].

Wt%	Al	Cu	Mg	Mn	Si	Fe	Ti
L8	95.57 ± 1.14	3.88 ± 0.05	0.83 ± 0.01	0.522 ± 0.007	0.60 ± 0.01	0.53 ± 0.04	0.063 ± 0.001
A-U4G [15]	base	4	0.7	0.5	0.5	0.5 max	0.2 max
2017A [11]	base	3.5–4.5	0.4–0.8	0.4–1.0	0.2–0.8	0.7	0.15
L2	94.30 ± 0.41	4.36 ± 0.03	1.53 ± 0.02	0.501 ± 0.006	0.167 ± 0.001	0.25 ± 0.01	0.0097 ± 0.0002
A-U4G1 [15]	base	4.25	1.5	0.7	0.4 max	0.5 max	0.2 max
2024 [11]	base	3.7–4.5	1.2–1.5	0.15–0.8	0.15	0.20	0.15

up to SiC 1000 grade in order to eliminate the painting and in some cases some irregular surface flatnesses. The thickness (direction D3) of the tensile test specimen is in the range of 1.2–1.5 mm. The tensile test was performed at a strain rate of 0.02 mm s^{-1}, on Synergie apparatus using a MTS® extensometer. For each plate, 8 gauges were measured.

2.2.4. Hardness

Microhardness measurements were carried out on each side of each

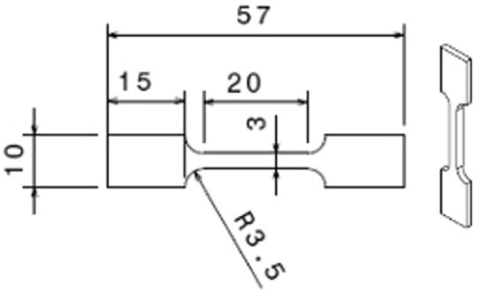

Fig. 2. Shape and dimension (mm) of the tensile specimen.

plate using a Buehler Omnimet serie 2100, applying a load of 300 g during 10 s on polished surfaces. Results are given in Hardness Vickers (HV) numbers.

3. Results

3.1. Metallurgical characterization

3.1.1. Metallurgical structure

Observation performed after chemical etching, revealed a typical structure linked to mechanical deformation. As shown in Fig. 3, the grains exhibit elongation both in the (D1, D3) and (D2, D3) planes. The values of grain sizes are given in Table 2. They exhibit a large variation around the average values.

It is revealed that the elongation ratio defined as length/width is higher than 2 for (D1, D3) and (D2, D3) planes in both plates, but more pronounced for L2 than for L8.

For L8, this may result from a cross-rolling of the plate, conducting to similar size grains in the (D1, D2) plane. This process involves changing the rolling direction (usually 90°) after each pass [20]. It reduces grain directional dependency of mechanical properties, residual stress and improve the formability of the metal. However, the use of such a process in 1959 by Breguet Compagny remains to be proven. For L2, the rolling direction corresponds most probably to the D2 direction for which a marked elongation of the grains is evidenced.

Furthermore, as given in Table 2, the average size values of the L8 grains are smaller by a factor 2–3 than those in L2 plate. The maximum elongation is about 45 μm for L8, while it is 114 μm for L2.

From the hardness measurements also reported in Table 2, the values of L8 and L2 plates are about 132 HV and 150 HV respectively. There is not an important difference between the different planes excepted that the external surface corresponding to rolling plane (D1, D2) exhibits lower hardness values.

Thus when comparing L8 with L2 plates, the L8 cross-rolled plate exhibits a lower grain size and a lower hardness. The difference in microstructure is linked to the mechanical deformation and to the thermal treatment applied. But the difference of mechanical properties (hardness) finds mainly its origin in the difference of composition in addition elements such as Mg in L2 plate (Table 1), as it will be discussed in analysis and precipitations section.

3.1.2. SEM observation and EDS analysis - constituent particles and equilibrium phases

Fig. 4 shows typical coarse intermetallic particles detected from backscattered electron image with SEM and quantified with EDS. The two alloys reveal a similar density of micro-particles (around 15,000 particles/mm^2) with a particle size ranging from 1 μm up to 18 μm in length.

Among the coarse intermetallic particles, the distinction between the insoluble constituent precipitates and the equilibrium precipitates is possible (Table 3).

In general, constituent particles are the coarsest and first particles formed during solidification of the aluminum alloy ingot [21]. They contain iron and/or silicon impurities. Their size depends on the solidification rate, the content in iron and silicon and the manufacturing process. Mostly insoluble during further heat treatments, they do not participate in the hardening process of the alloy. For the L8 plate (Fig. 4), the fractioned and irregularly shaped grey particles correspond to these constituent particles. Al, Cu, Fe, Mn and Si with various proportions were detected by EDS, which could indicate that they correspond to α-AlMnSi or α-Al(Fe,Mn)Si phases.

On L2 plate, the same types of particles (α-Al(Fe,Mn)Si) were found. Another type of particle, rich in Fe and Cu, was also detected that reveals the presence of Al_7Cu_2Fe phase. All these phases are expected insoluble constituent particles for 2024 or A-U4G1 alloys [22].

In Fig. 4, round and bright particles observed in the L8 plate can be readily identified as θ-Al_2Cu equilibrium precipitates. On the L2 plate, similar looking particles appear to be also θ-Al_2Cu and S-Al_2CuMg equilibrium precipitates. These two types of precipitates form during aging after a solution heat treatment and quenching. The possible precipitation sequences for Al-Cu-Mg alloys follow the following steps [1,23]:

$$\text{Supersaturated solid solution (SSS)} \rightarrow \text{GPzone} \rightarrow \theta'' \rightarrow \theta' \rightarrow \theta - Al_2Cu,$$
$$\rightarrow \text{GPBzone} \rightarrow S'' \rightarrow S' \rightarrow S - Al_2CuMg$$

with GP and GPB being Guinier-Preston and Guinier-Preston-Bagaryatsky respectively. θ′ and S′ are metastable phases forming upon artificial aging and whose presence leads to the maximum hardening state. Equilibrium precipitates (θ-Al_2Cu and S-Al_2CuMg) are larger and more widely spaced and form by transformation or coalescence of metastable precipitates.

The latter precipitation sequence leading to S-Al_2CuMg was of controversial matter until recently [5,24,25], particularly about the crystallographic structure of the lath shape S′′ and S′ phases. It is now believed that these two phases have a crystalline structure identical to the equilibrium S phase but with varying lattice dimensions [26]. The lath-shape metastable precipitates will be named S′ here for distinction with coarser particles detected by SEM.

In general, for an industrial Al-Cu-Mg alloy, such as ancient A-U4G and A-U4G1 alloys, the copper is in excess compared to the magnesium. Hence, the sequence of precipitation depends on the Cu/Mg ratio [27]. For Cu/Mg ratio between 4 and 8, the precipitation sequence leads to the formation of both θ-Al_2Cu and S-Al_2CuMg equilibrium phases. Precipitation sequence leading to S-Al_2CuMg is known to provide a higher hardening at room temperature than the one leading to θ-Al_2Cu. However, the sequence of precipitation depends also on the Mg/Si ratio [21,27]. When there is an addition of silicon in alloys, hardening precipitates such as Mg_2Si (β) or $Al_5Cu_2Mg_8Si_6$ (Q phase) can also appear during the hardening sequence [27].

Thus the difference observed between the L2 and L8 plates has to be directly linked to their different compositions (Table 1). For the L2 plate, the Cu/Mg ratio is equal to 2.9, which means that Al_2CuMg precipitates should be the principal hardening agent. The presence of θ-Al_2Cu precipitates and black precipitates rich in Al, Mg and/or Si indicates that the hardening process followed in this case several precipitation sequences.

The L8 plate contains less than 1 wt% of Mg and 0.6 wt% of silicon (against 0.167 wt% in L2), which corresponds to a Cu/Mg ratio equal to 4.7 and a Mg/Si ratio equal to 1.4. The precipitation in L8 is thus different than in L2. Because of the low Mg/Si ratio (< 1.7) in L8, S-Al_2CuMg precipitation sequence is not favorable: only Θ-Al_2Cu and $Al_5Cu_2Mg_8Si_6$ should be formed. In the L8 plate, the black particles observed by SEM, with a composition of Al(Cu)MgSi could correspond to this phase.

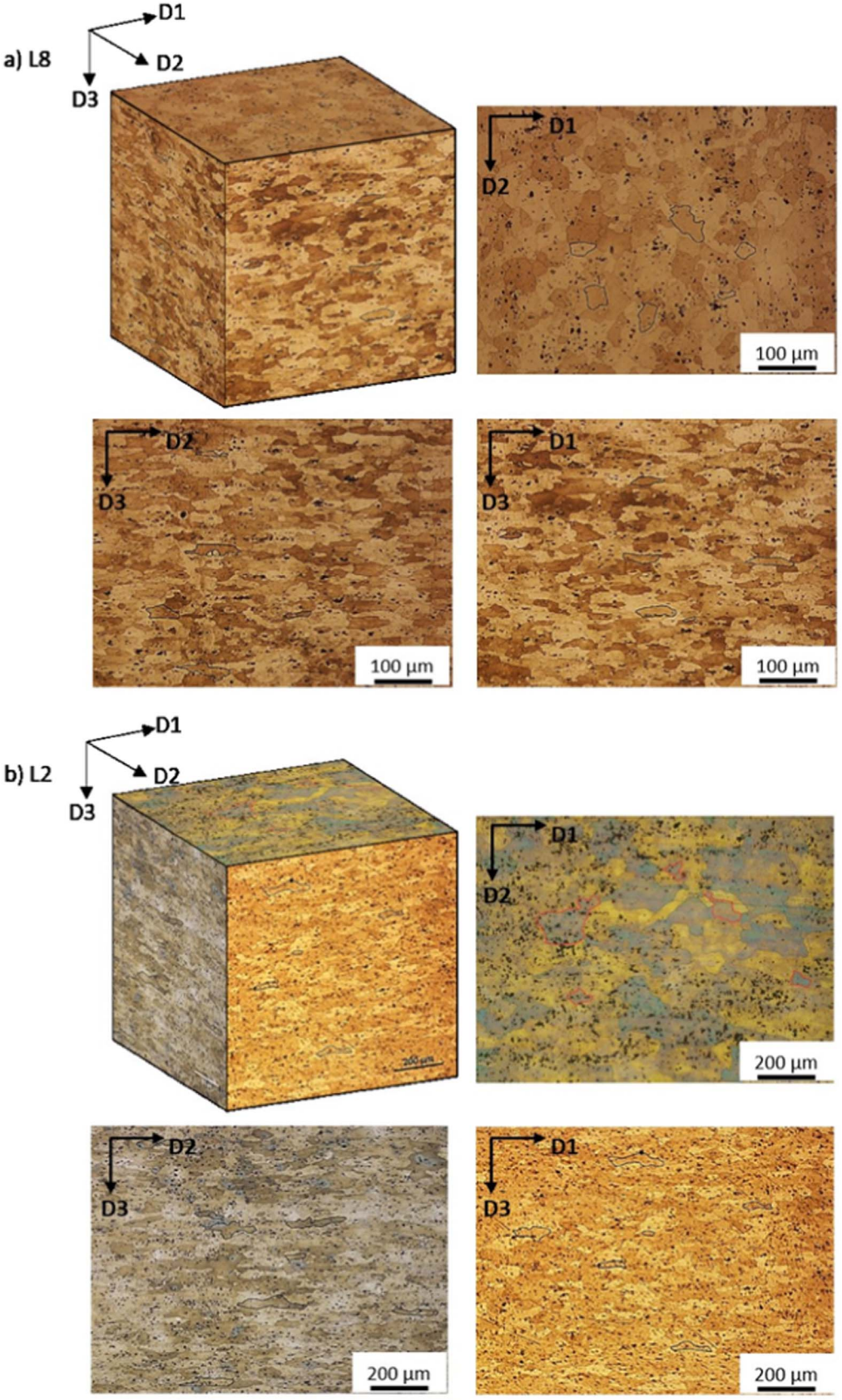

Fig. 3. Metallographic observation in the (D1, D2, D3) space – structure of (a) L8 and (b) L2 plates after etching (Keller solution).

Table 2
Grain sizes and hardness of L8 and L2 plates according to the (D1, D2, D3) space.

Plate number/ section	Microstructure - Global shape	Grain size (average ± std dev.)		Ratio L/ W	Number of measurements	Hardness (HV)	Number of measurements
		Length (μm)	Width (μm)				
Plate L8	**(average)**					**132 ± 7**	***75***
(D1, D2) external surface	Equiaxial	35 ± 9	30 ± 9	1.2	50	124 ± 3	20
(D1, D3)	Elongated	46 ± 15	15 ± 5	3.1	50	141 ± 8	15
(D2, D3)	Elongated	44 ± 24	19 ± 8	2.3	57	132 ± 5	40
Plate L2	**(average)**					**150 ± 7**	***75***
(D1, D2)	Elongated	98 ± 44	64 ± 28	1.5	40	147 ± 4	33
(D1, D3)	Elongated	69 ± 35	23 ± 8	3	40	161 ± 7	15
(D2, D3)	Elongated	114 ± 53	29 ± 12	3.9	40	149 ± 5	27

3.1.3. TEM analysis - nanostructure

3.1.3.1. Dispersoids and fine precipitation. Fig. 5 details typical submicronic particles identified with TEM and EDS. At this investigation scale, the two studied alloys reveal different particle shapes and sizes.

As regards to the submicronic scale, different rod-like precipitates are evidenced for L2 and L8 plates. For the L2 plate, having a composition close to 2024 alloy, the precipitates have a regular rod-like shape with a length in the range of 30–290 nm, mainly composed of Al, Cu and Mn and homogeneously distributed throughout the matrix. These particles, also called dispersoids, are formed during a long-term heat treatment, such as the ingot homogenization and have thereafter a low solubility in solid aluminum through some of their constituent elements: Cr, Mn and/or Zr. Their role is to control grains size and resistance to recrystallization avoiding large grains formation and favoring grain boundaries to pin dislocations [21]. For an alloy of 2024 type with a typical weight Cu/Mg ratio equal to 2.8, the main dispersoids expected are $Al_{20}Cu_2Mn_3$, so-called phase T [21,28].

Table 3
Precipitates identified by SEM-EDX and TEM-EDX within sampled aeronautic L8 and L2 plates.

	L8 A-U4G	L2 A-U4G1	Literature known precipitates
Hardening phase	AlCu	AlCu	θ'-Al_2Cu [23]
Equilibrium phase	AlCu	AlCu	θ-Al_2Cu [23]
		AlCuMg	S-Al_2CuMg [23]
Constituent phases	Al(Cu)MgSi	Al(Cu)MgSi	$Al_5Cu_2Mg_8Si_6$ [27]
		AlCuFe	Al_7Cu_2Fe [22]
	Al(Cu, Fe, Mn, Si)	Al(Cu, Fe, Mn, Si)	$Al_{12}(Fe, Mn)_3Si$ [22]
Dispersoids	AlMn(Fe)Si	AlCuMn	$Al_{20}Cu_2Mn_3$ [28]

In the L8 plate, ovoid and rod-like shape particles with length and width varying from 40 to 200 nm are observed, thus smaller than the

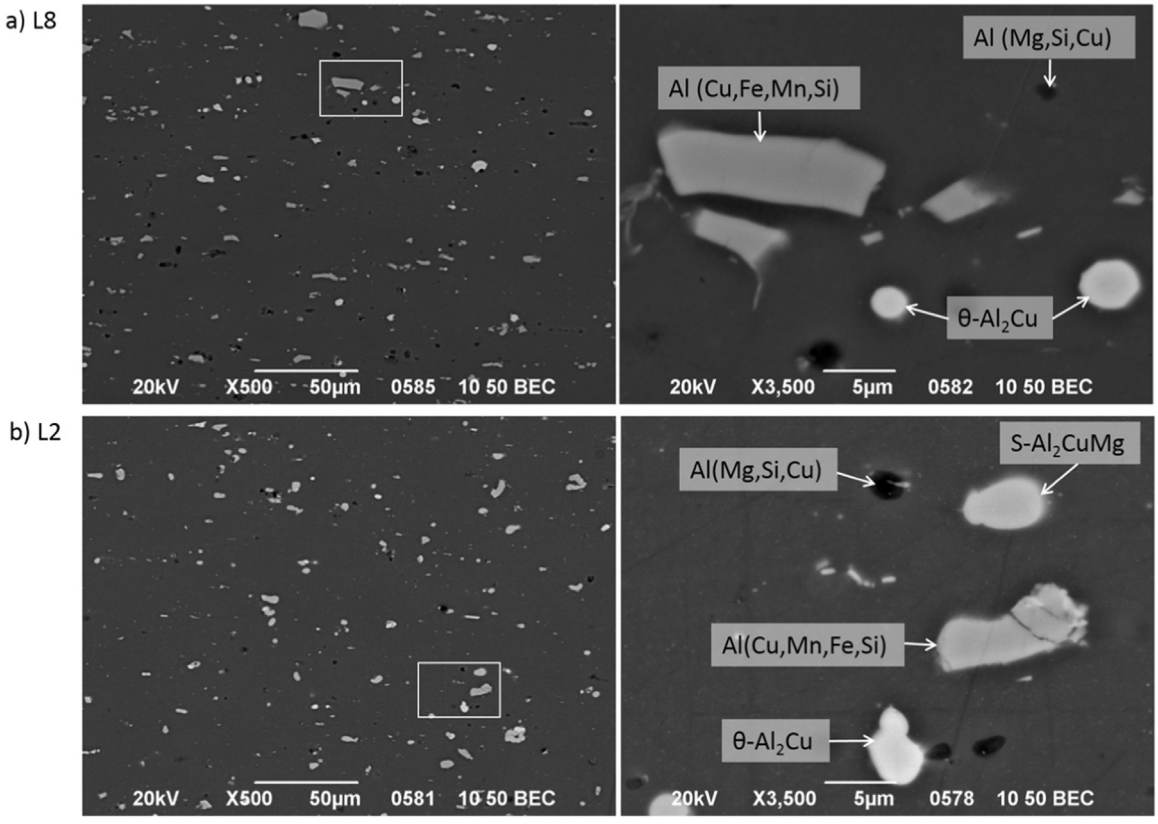

Fig. 4. Constituent particles and equilibrium phases identified by SEM with backscattering detector and EDS, (a) on L8 plate: θ-Al_2Cu, Al(Cu,Fe,Mn,Si), Al(Mg,Si,Cu); (b) on L2 plate: θ-Al_2Cu, S-Al_2CuMg, Al(Cu,Fe,Mn,Si), Al(Mg,Si,Cu).

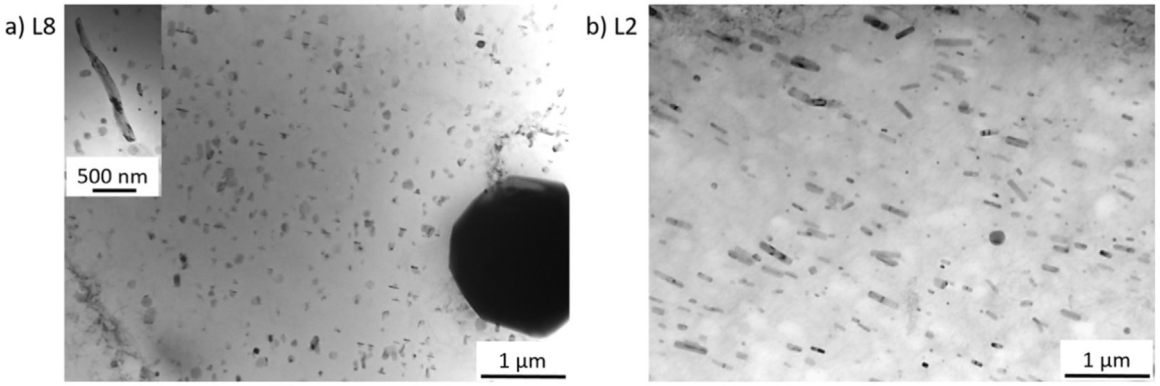

Fig. 5. Dispersoids observed by TEM for samples in the rolling plane (D1,D2), (a) on L8 plate, with grain boundary precipitation (inset) and SiO_2 faceted particle, (b) on L2 plate.

dispersoids detected in L2, and sometimes aligned along perpendicular axes. With TEM-EDS, it is noted that the composition of particles is quite heterogeneous: AlMnFeSi, AlMnSi, AlCuFe and AlCuMgSi can be found. In this case, the dispersoids are supposed to be the ones containing Mn: of the type AlMnSi or AlMnFeSi. As shown on Fig. 5(a), precipitation at grain boundaries (inset) is observed. SiO_2 faceted particles are also quite often found due to high silicon rate in this A-U4G alloy.

As regards to the nanometric level, in L8 and L2 plates, smaller particles with round shape in the range of 5 and 20 nm and heterogeneous distribution were observed (Fig. 6).

Composed of mainly Cu, these small size intermediate particles participate in hardening. Dislocations are indeed pinned by these small size particles, which proves that they contribute to the hardening of the material by hindering the movement of dislocations. These type of small particles observed in both plates can also be found in equivalent modern 2024 alloys with a T3 temper [5,29].

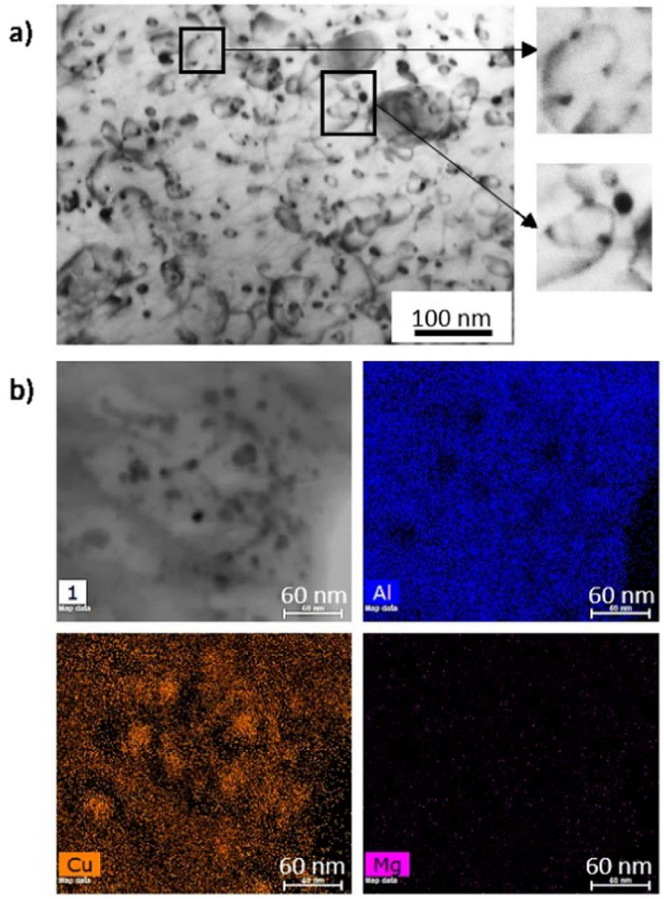

Fig. 6. Small-size particles and dislocations observed by TEM on L2 with EDS mapping showing the copper rich nature of particles.

In L2 piece (A-U4G1), whose precipitation is supposed to be conducted mainly via S-type phase, the hardening S′-phase in the form of laths was not found. As explained in [1,29], for wrought alloys tempered at room temperature, corresponding to T4 in modern designation of treatments [14], precipitation is exclusively GPB, which is not observable with conventional TEM. Semi-coherent and coherent precipitates, metastable S′-phase, with a lath shape appear generally upon artificial aging (corresponding to T6 or T8 treatment) as shown in [14,26,29,30].

Table 3 summarizes the various particles found in the two plates at different observation scales, including a comparison with known precipitates from literature.

3.1.3.2. Dislocations. An important feature concerns dislocations microstructure and localization as they could give indication on the mechanical and heat history experienced by each piece. A lot of dislocations were observed by TEM in the two plates, as shown in Fig. 7.

In the L2 plate, the dislocations surround the dispersoids. In the L8 plate, however, the dislocations distribution and type are not exactly the same: helical type dislocations loosely distributed in the matrix are observed. This generally happens when heat is applied and dislocation climb is activated [31], and could be a sign of aging linked to the flight period of the aircraft.

3.2. Mechanical characterization

Mechanical tests performed on L8 and L2 plates revealed a very good reproducibility of the tensile strength curves. This is observed both on the D1 direction as well as on the transversal one D2.

A typical curve for each rolling directions is given in Fig. 8. The measured mechanical properties are given in Table 4, together with data from archives discussed hereafter. For the two plates, the Young modulus and the rupture strain are equivalent: around 67 GPa and 16% respectively. However, an important difference is found concerning the strength properties. It is higher for L2 than for L8. This agrees well with the microstructure patterns and hardness values previously evidenced. As a consequence, the alloy of the L2 plate exhibits higher mechanical properties than that of L8.

Although the grain size is more important for L2 than for L8, the reason for higher mechanical properties comes from the higher Mg rate, which is known to increase the tensile strength and hardness of Al-Cu alloys [23].

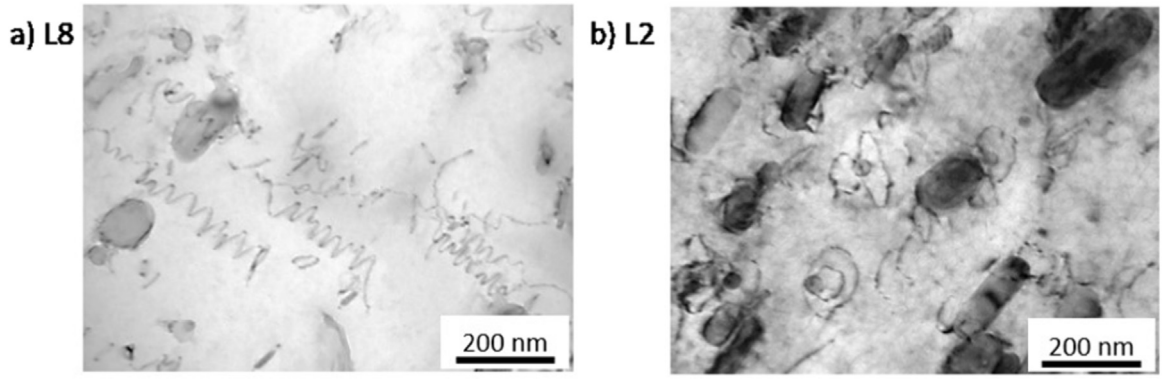

Fig. 7. Dislocations observed by TEM on (a) L8 and (b) L2 plates.

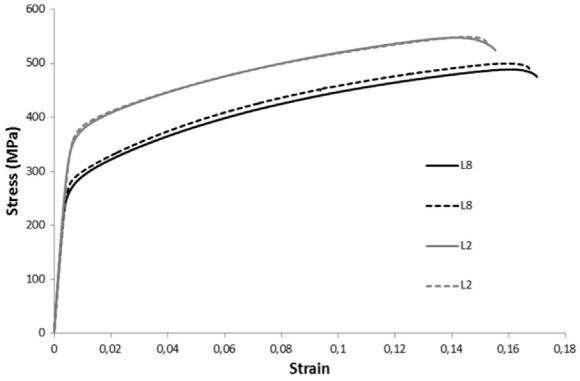

Fig. 8. Tensile strength curves for L8 and L2 plates. Full lines are for specimen parallel to the rolling direction D1 and dashed line are for the other rolling direction D2.

4. Discussion

4.1. Comparison of mechanical properties: after natural aging vs original informative data

The mechanical properties extracted from measurements of L8 and L2 plates are summarized in Table 4. They were compared to historical data extracted from archives documents. Table 4 also presents the standard values recommended by Breguet's aircraft company in 1957, together with a range of values for the same alloys reported in 1954 by a generalist French scientific and technical journal: la Revue de l'Aluminum [32]. Current standards data for commercial 2017A-T4 and 2024-T4 alloys are also given for reference [33].

The first observation is that the measured yield strength, ultimate strength and rupture strain for L8 (A-U4G) and L2 (A-U4G1) are consistent with the company's standards [16] and fall in the expected range for applications broader than aeronautics. The materials recovered from the Breguet 765 are close to current standards for 2017A-T4 and 2024-T4.

Although the original state of these particular parts remains unknown, one can say that after 10 years of flight service and 47 years of outdoor conditions, uncorroded zones of the alloys in use in the Breguet Sahara kept the required mechanical properties.

These results complement studies reported in the literature on naturally aged alloys directly sampled from aircrafts at the end of their usage life. Salimon et al. [34] proved indeed that bulk material 2024-T4 remained unaffected mechanically by the high cycle fatigue experienced during 11–20 years of service. Changes in chemical composition and in the structure were confined to a thin surface layer making the material more sensitive to corrosion.

However, in our study a difference is noticed concerning the hardness. The values of 132 ± 7 HV for L8 (A-U4G) and 150 ± 7 HV for L2 (A-U4G1) are significantly higher than the recommended and standards values, respectively 117 HV and 129 HV. This marked difference could be related to a work hardening process occurring during the lifetime of the aircraft.

4.2. Effect of long-term aging – structural correlation

For both alloys, A-U4G1 (L2) and A-U4G (L8), most microscopic constituent particles, mesoscopic dispersoids and nanometric hardening precipitates were identified.

Table 4
Mechanical properties determined from tensile tests of L8 and L2 plates and corresponding Al-Cu-Mg alloys properties from Breguet Standards (1954) [16], Revue de l'Aluminium (1954) [32] and recent handbook [33].

		Young modulus Kg/mm² (GPa)	Yield strength Kg/mm² (MPa)	Ultimate strength kg/mm² (MPa)	Rupture strain	Hardness HB[a]/HV
Measurements (this work)	**L8 plate**	6830 (67)	27 (264)	43 (421)	17%	113/132
Breguet standards (1957) [16]	**A-U4G 495 °C Matured for 4 days (sheet)**	7000 (69)	27 (265)	40 (392)	15%	100/117
Revue de l'Aluminium (1954) [32]	**A-U4G**	–	26–45 (255–441)	43–54 (422–529)	11–25%	–
Kaufman (2008) [33]	**2017A-T4**	7342 (72)	28 (275)	43 (425)	22%	105/123
Measurements (this work)	**L2 plate**	6730 (66)	35 (348)	49 (477)	15%	127/150
Breguet standards (1957) [16]	**A-U4G1 500 °C Matured for 4 days (sheet)**	7000 (69)	32 (314)	45 (441)	15%	110/129
Revue de l'Aluminium (1954) [32]	**A-U4G1**	–	31–46 (304–451)	44–58 (431–569)	10–21%	–
Kaufman (2008) [33]	**2024-T4**	7444 (73)	33 (325)	48 (470)	19–20%	120/141

[a] Calculated according to standard ASTM designation E 140: HB=3.76211+0.825368 (HV) for wrought aluminum alloys.

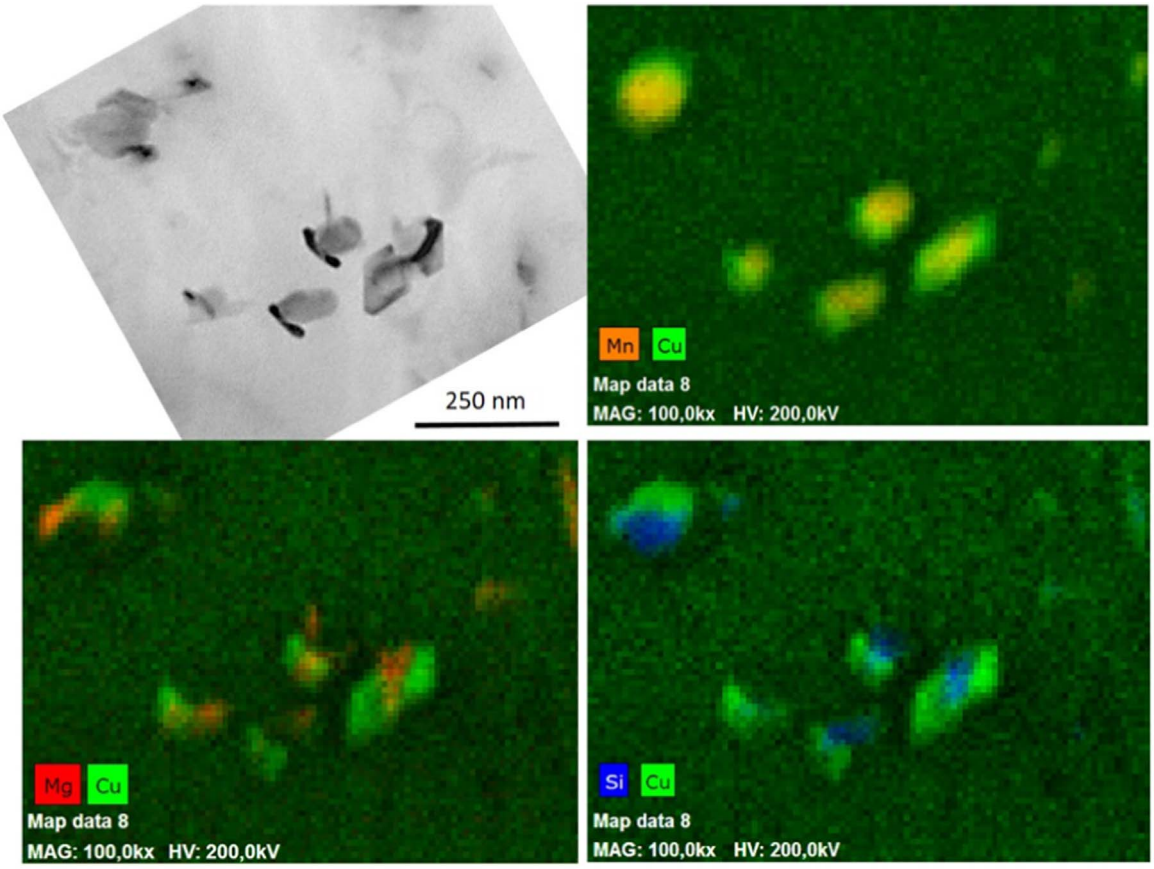

Fig. 9. TEM-EDS mapping on L8 plate showing the nature of precipitates nucleating on intermetallic type particles.

In L2 sheet, they correspond, in nature, shape and distribution to what is expected for 2024-T4 [1,5,29]. Treatment T4 is identical to the treatment described in Breguet's standards [16]: tempered for 4 days at room temperature. The similarity in matrix precipitates in L2 with literature data is consistent with the mechanical properties here measured.

For A-U4G (L8 plate), precipitates nature and distribution were also identified. We noticed a very heterogeneous distribution of compositions for dispersoid-type particles, which is probably linked to the higher impurities level (Si and Fe mainly) in L8 compared to L2 plate. It is however difficult to make rational comparisons with literature. The modern equivalent alloys (2017A) are not as thoroughly observed with TEM as 2024 alloys, and as regards to scientific literature from the 50s or 60s, there was no similar study to be found as electron microscopy was not at that time being extensively applied for industrial alloys. Saying that, some peculiar features were observed on L8 plate, as detailed in Fig. 9: precipitation of Mg-rich particles on dispersoids (AlMnSi type) which act as nucleation sites. This can appear upon heating [4,30], and it is worth recalling that L8 was a flame-shield plate located inside the engine nacelle, thus subjected to higher temperatures than L2. To validate this point, additional investigation was performed on another A-U4G piece also sampled on the same airplane, but which didn't experience any heating from the engine. This Al-sample is a flat collected on the inner desk part of the Breguet 765. In this sample, the re-precipitation phenomenon was not observed as shown in Fig. 10.

Furthermore, for the L8 plate, several other observations at the nanoscale indicate that the plate experienced some heating. In particular, helical-type dislocations have a loose distribution (Fig. 7), compared to the case of L2 where dislocations are pinned by dispersoids. Another peculiar feature is the numerous precipitates with elongated shape at grain boundaries as shown in Fig. 5(a). The temperature and the exposure time experienced by the L8 plate are unknown but some assumptions can be made. The temperature probably didn't exceed 150 °C since no needle shape (θ'-Al_2Cu) or lath shape (S′-phase) precipitation occurred. On the other hand, it is highly possible that the plate experienced temperatures higher than 80 °C as microstructural changes were detected. In [6] indeed, no microstructural changes were observed in 2024 alloys for exposure times equivalent to about 100,000 h at 80 °C, which is a much longer time than the lifetime of the Breguet Sahara. It can be estimated indeed that the Breguet 765 Sahara n°504 flew a maximum of 36, 500 h based on the hypothesis that the flight-time was 10 h per day for 10 years of service. In the present case, observed microstructural changes occurred due to exposure to temperature higher than 80 °C.

However, despite the nanoscale changes in microstructure here evidenced, the mechanical properties for L8 alloy remain adequate to the initial company's specifications. They might have evolved with time. For proving this assumption, one would need to measure the mechanical properties of the original material.

To explain the higher hardness in both alloys, further investigation should be conducted, in particular quantitative studies on precipitates size and on dislocation density.

5. Conclusion

Even if aluminum alloys and related fabrication processes were developed relatively recently in industry, parts recovered from old aircrafts can provide a lot of information useful for the field of material science. Two vintage aluminum alloys, A-U4G and A-U4G1 in the form of plates were recovered from a Breguet 765. Multi-scale observations of their microstructure and mechanical tests allowed the understanding of their nature and fabrication process. It was indeed possible to confirm:

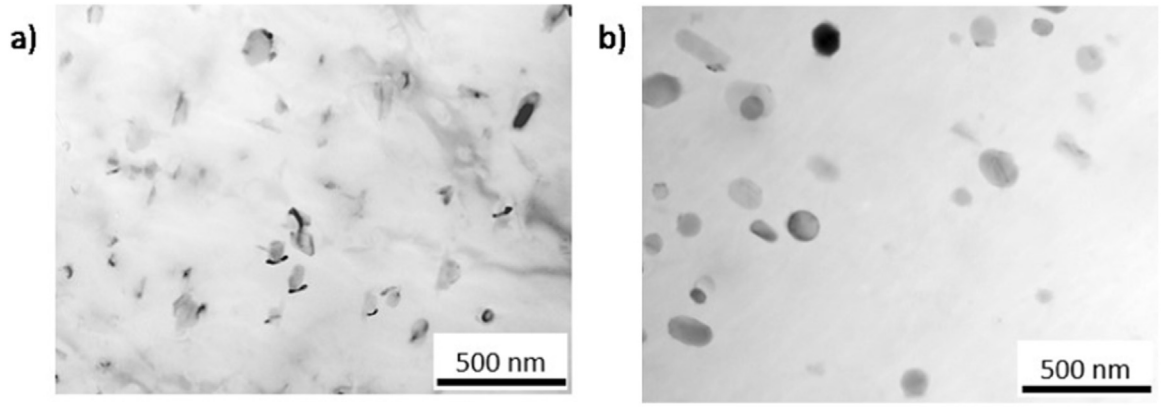

Fig. 10. TEM images of dispersoids (a) on L8 and (b) on unheated A-U4G piece from the Breguet 765 Sahara n° 504 showing that re-precipitation observed is specific to L8.

- The nature of the alloy thanks to chemical analysis but also thanks to TEM observation pointing out specific precipitation phases.
- But also several fabrication steps:
- The mechanical treatment, *i.e.* rolling, thanks to the observation of grain size and orientation.
- The age-hardening treatment thanks to the observation of the presence or absence of hardening precipitates. S′-type hardening precipitates in the form of laths were not observed which confirms that the alloys were matured (T3 or T4 temper) and not artificially aged (T6 or T8 temper). Nano-size copper-rich precipitates pinning the dislocations are similar to ones recently observed in 2024-T3 alloys.

Most interesting, the alloys were naturally aged for about 60 years: 10 years experiencing flights cycles of the aircraft and more than 47 years outdoors without flying. It is shown that both alloys kept good mechanical properties, conformed to standards and most probably close to their original state. Hardness was however significantly increased and this remains to be explained.

Some structural changes were observed at the micro- and nano-structure levels for one of the plate (L8 – A-U4G alloy). They are related to the conditions experienced by the plate during the lifetime of the aircraft. This plate located close to the engine most probably experienced some increased temperature. But despite this service aging (temperature cycles, mechanical strain for 10 years) and although signs were detected at the nanoscale, there is no evident change in the mechanical properties at macroscale. It would be interesting to measure the mechanical properties and especially the hardness of the same alloys in a state close to the original state (such as spare-parts kept for this aircraft) to determine a more precise aging of the material.

The presented results show that studies of naturally-aged alloys could thus be considered to complete artificial aging tests for evaluating the long-term aging of structures. Future experiments will consist in comparing the microstructure of these ancient alloys to artificially aged modern alloys (such as recent 2017A-T4 and 2024-T4).

Acknowledgements

This work was supported by RTRA (Réseau Thématique de Recherche Avancée) - Science and Technologies for Aeronautics and Space, through the VIMA project (Aging of Advanced Materials), by doctoral fellowship PRES (Ref. 5913)/ Région (Ref. 12053330) through the MIPROPAL project and by Programme Investissements d'Avenir under the program ANR-11-IDEX-0002-02, reference ANR-10-LABX-0037-NEXT.

The authors would like to thank the association *Ailes Anciennes Toulouse*, especially the team “Breguet-2 ponts” for providing the samples and precious information on the aircraft. Dominique Lamirault of the preparation service at CEMES for the thin slices used in TEM is also warmly acknowledged.

References

[1] E.A. Starke Jr., Heat-treatable aluminum alloys, Aluminum Alloys–Contemporary Research and Applications 31, Academic Press, Inc., San Diego, CA, 1989, pp. 35–65.
[2] G.E. Totten, D.S. MacKenzie (Eds.), Handbook of Aluminum, Physical Metallurgy and Processes, CRC Press, Basel, Marcel Dekker, New York, vol. 1, 2003.
[3] National Research Council, Accelerated Aging of Materials and Structures: The Effects of Long-Term Elevated-Temperature Exposure, The National Academies Press, Washington, DC, 1996, p. 65.
[4] M. Wiersbinska, J. Sieniawski, The influence of long-lasting annealing on micro-structure of AlCu4Ni2Mg2 alloy, J. Achiev. Mater. Manuf. Eng. 34 (2009) 122–129.
[5] C.K.S. Moy, M. Weiss, J. Xia, G. Sha, S.P. Ringer, G. Ranzi, Influence of heat treatment on the microstructure, texture and formability of 2024 aluminium alloy, Mater. Sci. Eng.: A 552 (2012) 48–60.
[6] C. Larignon, Mécanismes d'endommagement par corrosion et vieillissement microstructural d'éléments de structure d'aéronef en alliage d'aluminium 2024-T351, Doctorat de l'Université de Toulouse, Institut National Polytechnique de Toulouse, 2011.
[7] R. Braun, C. Juricic, G. Tempus, Mechanical properties and corrosion behaviour of 2024-T351 sheet thermally exposed at slightly elevated temperatures, Progress in Mechanical Behaviour of Materials (Icm8), Vol 2: Material Properties, 1999, pp. 597–602.
[8] N.D. Alexopoulos, P. Papanikos, Experimental and theoretical studies of corrosion-induced mechanical properties degradation of aircraft 2024 aluminum alloy, Mater. Sci. Eng. A 498 (2008) 248–257.
[9] V. Guillaumin, G. Mankowski, Localized corrosion of 2024 T351 aluminium alloy in chloride media, Corros. Sci. 41 (1998) 421–438.
[10] J. DeDamborenea, A. Conde, Comparison of accelerated and atmospheric exposure tests for corrosion of aluminium alloys, Br. Corros. J. 30 (1995) 292–296.
[11] The Aluminum Association, International alloy designations and chemical composition limits for wrought aluminum and wrought aluminum alloys. ⟨http://www.aluminum.org/resources/industry-standards/aluminum-alloys-101/⟩, 2015 (Accessed 12 April 2016).
[12] A. Cochard, J. Douin, B. Warot-Fonrose, J. Huez, L. Robbiola, J.-M. Olivier, P. Sciau, Benefits of the complementary use of archaeometry investigations and historical research in the study of ancient airplanes: the Breguet Sahara's rivets, in: M.R. Society (Ed.) MRS Fall Meeting, vol 1656, Cambridge University Press, Boston, 2013, pp. 1–10.
[13] J. Cuny, P. Leyvastre, Les avions Breguet (1940–1971), 2e partie, ed. Larivière, Coll. Docavia, Paris, 1973–1977, pp. 75–79.
[14] E.A. Starke Jr, J.T. Staley, Application of modern aluminum alloys to aircraft, Prog. Aerosp. Sci. 32 (1996) 131–172.
[15] Tableaux des alliages d'aluminium et des alliages de magnésium, norme AIR 3350/C, édition n°4 du 15 juin 1957, Ministère de la Défense Nationale et des Forces Armées, Secrétariat d'Etat aux Forces Armées (AIR), Direction Technique et Industrielle, édition n°4 du 15 juin 1957, p. 5.
[16] Fiche Standard Br. 201, feuille 1, Usine d'Anglet, MINDEF - Service historique de la défense, Châtellerault, édition Février 1956 et janvier 1957, p. AA 416 2C5 199.
[17] Service Technique de l'Aéronautique – section Avions, Clauses Techniques Breguet 765, Centre de Documentation du Musée de l'Air et de l'Espace du Bourget, 1956.
[18] O.H. Duparc, Alfred Wilm et les débuts de Duralumin, Cahiers d'histoire de l'aluminium, Institut pour l'Histoire de l'Aluminium 63-77, 2005.
[19] Alcoa, 2024 Aluminum Alloy Sheet and Plate. ⟨www.alcoa.com/mill_products/north_america/en/product.asp?Prod_id=595⟩, 2016 (Accessed 31 May16).
[20] M. Rout, S.K. Pal, S.B. Singh, Cross rolling: a Metal Forming Process, in: J.P. Davim (Ed.)Modern Manufacturing Engineering, Springer International Publishing, Cham, 2015, pp. 41–64.
[21] S.C. Wang, M.J. Starink, Precipitates and intermetallic phases in precipitation hardening Al-Cu-Mg-(Li) based alloys, Int. Mater. Rev. 50 (2005) 193–215.
[22] J.R. Davis, Aluminum and Aluminum Alloys, Materials Park, ASM International, Ohio, 1993.
[23] B. Dubost, P. Saintfort, Durcissement par précipitation des alliages d'aluminium,

Techniques de l'Ingénieur M240, 1991, pp. 2–4.
[24] S.C. Wang, M.J. Starink, Two types of S phase precipitates in Al–Cu–Mg alloys, Acta Mater. 55 (2007) 933–941.
[25] M.J. Styles, C.R. Hutchinson, Y. Chen, A. Deschamps, T.J. Bastow, The coexistence of two S (Al2CuMg) phases in Al–Cu–Mg alloys, Acta Mater. 60 (2012) 6940–6951.
[26] G. Sha, R.K.W. Marceau, X. Gao, B.C. Muddle, S.P. Ringer, Nanostructure of aluminium alloy 2024: segregation, clustering and precipitation processes, Acta Mater. 59 (2011) 1659–1670.
[27] L.F. Mondolfo, Aluminum Alloys, Structure and Properties, Butterworths, London-Boston, 1976.
[28] Z. Shen, C. Liu, Q. Ding, S. Wang, X. Wei, L. Chen, J. Li, Z. Zhang, The structure determination of $Al_{20}Cu_2Mn_3$ by near atomic resolution chemical mapping, J. Alloy. Compd. 601 (2014) 25–30.
[29] Y.C. Lin, Y.-C. Xia, Y.-Q. Jiang, H.-M. Zhou, L.-T. Li, Precipitation hardening of 2024-T3 aluminum alloy during creep aging, Mater. Sci. Eng. A 565 (2013) 420–429.
[30] R. Alani, M. Pan, In situ transmission electron microscopy studies and real-time digital imaging, J. Microsc.- Oxf. 203 (2001) 128–133.
[31] J. Friedel, Dislocations, Pergamon Press, 1964, p. 122 (Chap. 5.4).
[32] R. Chevigny, L'aluminium et ses alliages, Revue de l'Aluminium, Paris, vol. 211, 1954, p. 175.
[33] J.G. Kaufman, Properties of Aluminum Alloys, Fatigue Data and the Effects of Temperature, Product Form and Processing, Materials Park, ASM International, Ohio, 2008.
[34] S.R. Salimon, A.I. Salimon, K. A.M, The evolution of electrochemical, microstructural, and mechanical properties of aluminium alloy 2024-T4 (D16AT) during fatigue cycling, Proceedings of IMechE (Part G)J. Aerosp. Eng. 224 (2010) 339–353.